TECHNICAL MEMORANDUMS

NATIONAL ADVISORY COMMITTEE FOR AERONAUTICS

No. 910

MEASUREMENTS ON A LOW-WING MODEL IN THE ROTATING JET AND COMPARISON WITH FLIGHT MEASUREMENTS

By W. Bader

Luftfahrtforschung
Vol. 16, No. 2, February 20, 1939
Verlag von R. Oldenbourg, München und Berlin

Washington
September 1939

NATIONAL ADVISORY COMMITTEE FOR AERONAUTICS

TECHNICAL MEMORANDUM NO. 910

MEASUREMENTS ON A LOW-WING MODEL IN THE ROTATING JET AND COMPARISON WITH FLIGHT MEASUREMENTS*

By W. Bader

SUMMARY

The present report deals with six-component measurements in the small tunnel of the DVL on a model of the BFW-M $27b_1$, which were made to determine the effect of rolling and yawing on the air forces and moments. The experiments were carried out in a rotating air stream. The wind was given a spiral motion by means of a rotating screen, the model being suspended in the conventional manner.

From the findings, the following points are of special interest:

1) With markedly increasing angles of yaw the maximum lift shifts to higher angles of attack;

2) At lower angles of attack the drag is reduced during rolling;

3) In the stalling range the drag is increased during rolling;

4) At high angles of attack the lateral force shows a reversal of sign; the effect of rolling on the lateral force is quite considerable;

5) The pitching moment appears to be relatively independent of rolling;

6) The yawing-rolling moment is very high in the region well beyond stalling.

---

*"Messungen an einem Tiefdeckermodell in rotierenden Strahl und ihr Vergleich mit Flugmessungen." Luftfahrtforschung, Bd. 16, Lfg. 2, pp. 104-111.

The lack of accuracy in the measurement of the rolling-yawing moments was disturbingly noticeable.

For comparison with the model tests, several spin tests were made in an airplane; the extrapolations, effected with certain reservations, indicate that the employed test method of rotating air stream affords in many cases a practical means for the relatively simple prediction of the effect of rolling on the air loads and moments with a good degree of accuracy.

INTRODUCTION

In the last few years the air loads and moments at high angles of attack have received considerable attention, especially in British and U.S. research laboratories. Since in those problems it concerns first of all the effect of rotation about the wind axis at different angles of attack and yaw, the execution of the experiments, generally on the so-called spinning balance, present in part considerable difficulties. The fundamental advantage of this type of experiment is this: In free flow the static pressure is constant and the boundary layer can, if necessary, follow, in the same manner as on the spinning airplane, the centrifugal force.

In spite of the great amount of data available it is still far from possible to predict, even approximately exact, the course of the aerodynamic quantities without measurements in a given particular case. Since, at the time of the test flights with a low-wing monoplane of the BFW-M $27b_1$ type, the wish for more accurate information about the aerodynamic behavior of the airplane had been voiced, it was decided to make some wind-tunnel tests with the new spin recording device developed by Kramer and Krüger (reference 1). These measurements are recounted hereinafter: First, it was intended to verify to what extent the view, expressed in the literature, of the independence of the forces from the rotation, important in the mathematical treatment of the spinning problem, holds true in the present case. In particular, the course of the lateral force in relation to angle of attack, angle of yaw, and rotation were to be determined with a view to more accurate information about the angle of yaw of the relative wind. On account of the known difficulties in the prediction of the aerodynamic moments, the experiments

were to explain the question deciding the usefulness of the method whether or not the effect of the different influential quantities is correctly reproduced in model testing.

In the new spinning balance the model is suspended from the conventional six-component balance in the tunnel jet which is given a spiral motion by a rotating screen. This type of experiment has, from the recording point of view, fundamental advantages over the operation on the spinning balance; but, as pointed out at the same time by Kramer and Krüger, it also has one fundamental defect: the static pressure of the free flow is not constant. As a result of the centrifugal force applied at the jet the static pressure decreases a little according to a parabolic law from the circumference to the jet center. Measurements disclosed a very close accord between theory and experiment.

The moments induced by the variable static pressure themselves may, at higher angles of attack where the tail is perceptibly away from the jet center, be ignored in the face of the elsewhere existing instrumental inaccuracies. Another question is whether, as a result of the pressure gradient, a movement of the boundary layer might occur which could effect a substantial change of profile characteristics. This change would be in the opposite sense from the flight test. Since, on the other hand, the speed of jet rotation in the tests was fairly low and furthermore, the drop in static pressure at jet center remained small, no appreciable effect on the profile characteristics through boundary-layer movement was anticipated.

TEST PROCEDURE

In view of the original intention to include measurements with the introduction of a spinning radius, the model was made comparatively small. The lessened instrumental accuracy resulting therefrom was, to a certain degree, ameliorated through the use of sufficiently sensitive metering diaphragms. This was most difficult to achieve in the drag component measurements where, because of the smallness of the righting forces, it was difficult to get an exact reading of the zero reference values. Another drawback resulting from the smallness of the model was that the

value of $\lambda = \frac{\Omega s}{v}$ could not increase excessively in the experiments. The best way for obtaining high speeds would have been with high angular velocities at sufficiently high tunnel speeds, in order to run the test at the largest possible Reynolds Numbers.

On account of the severe speed decrease due to the rotating screen, it was impractical to raise the dynamic pressure above 30 kg/m², the maximum wind-tunnel speeds used in spinning-balance tests, at which the strength of the model and incipient oscillations form an upper dynamic pressure limit.

At this first trial of the new arrangement, the highest dynamic pressure could not yet be utilized in spite of various improvements, because of difficulties with the rotating screen, which, for lack of time, could not be remedied. Measurements made for maximum-lift appraisal at 15, 20, and 25 kg/m² dynamic pressures manifested, in agreement with other investigations, no appreciable influence of the Reynolds Number in this range; as a result the tests were in general run at the low dynamic pressure of 15 kg/m². The choice of low tunnel speeds made it possible to obtain fairly satisfactory rotation values and hence of the effect of rotation on the loads and moments.

Since, in view of the difficulties, readily removed in subsequent tests with the rotating jet, the Reynolds Number was disproportionately small, it was attempted to increase the equivalent Reynolds Number by means of a turbulence grid built up of parallel round bars. It could not be mounted downstream from the rotating screen, as it would have destroyed part of the created turbulence. A turbulence grid made of radial bars which would have to be solidly mounted on the rotating screen would obviate this difficulty.

Lacking a hot-wire anemometer, the turbulence measurements were made with a calibrating sphere (140 mm diameter). They gave a turbulence factor of 2.7 for the non-rotating jet and a much lower figure for jet rotation (at a jet rotation of $n = 2.5\ s^{-1}$, it dropped to around 2). However, it is very likely that the still somewhat crude test method is unsuitable for the rotating jet. The effective Reynolds Number at 15 kg/m² dynamic pressure was 7.3×10^4 (reference length: mean wing chord).

The dynamic pressure was explored in the tunnel section passing through the axes of lift and lateral force; following several improvements it could be kept quite uniform. Although the distance of the cited tunnel plane from the turbulence grid amounted to about 70 times the thickness of one grid wire, the dynamic pressure still proved to be greatly affected by the grid and manifested a wavelike aspect along one tunnel diameter. This called for careful mounting of the dynamic pressure recorder, comprising three parallel Prandtl tubes whose position in the free stream had been so determined from previous tests that their readings gave the mean dynamic pressure with sufficient accuracy.

On account of the great mass inertia of the rotating screen, it was experimentally easier to plot a polar curve with fixed screen rotation and fixed angle of yaw than to change the rate of jet rotation at constant angles of flow. With the chosen test procedure a complete six-component measurement took only about 10 minutes. This time interval could not be exceeded, without overheating the screen rollers, causing their destruction amid violent vibrations in the tunnel nozzle.

A certain drawback of this test method is that the relation of the moments to jet rotation is obtained at first in parameter presentation and every section placed through experimentally obtained curves has in itself a certain uncertainty.

Figure 1 shows the test arrangement with model mounted, the rotating screen, turbulence grid, and anemometer used for predicting the speed of rotation of the jet can be seen in the background.

Most accurate geometric similarity based on comparative measurements with the experimental airplane was striven for on the 20:1 scale wooden model. It was fitted with adjustable lateral and horizontal controls, but not with ailerons. In agreement with this, the ailerons in the flight tests were set at zero. No propeller was fitted, especially since the flight tests were made at engine r.p.m. at which the propeller produced neither appreciable thrust nor drag.

The highly tapered wing section has a taper ratio of $l_a:l_i = 0.33$; an aspect ratio of $\Lambda = 9.5$, angle of twist

of about 4° and a 5° dihedral. In the first third of the semispan (counted from plane of symmetry) the airfoil is a Göttingen Gö 681; the other profiles over the mean line are thickened and flattened, respectively. A few data are reproduced for comparison with N.A.C.A. findings: maximum camber about 4.5 percent; backward position of maximum camber about 40 percent of the chord; thickness about 7 percent; which places the airfoil between 4417 and 5417 of the N.A.C.A. series.

SYMBOLS

The axes and angles are defined in figure 2. They correspond to the latest FALU standard of nomenclature. The angles in figure 2 are plotted positive; the arrows indicate the point from which the angles are counted. A positive angle of yaw indicates an advance of the starboard wing; thus a positive value of angle of yaw in a right spin indicates that the airplane is in an outward slip. While lift and drag coefficient are counted positive, as usual, for lift and drag in negative z_a or x_a direction, the lateral force is positive if in direction of the positive y_a axis. The moments, L, M, and N, are positive for positive rotation about their respective axes.

The moment coefficients are defined as

$c_L = \frac{L}{qFs}$, rolling moment;

$c_M = \frac{M}{qFl}$, pitching moment;

$c_N = \frac{N}{qFs}$, yawing moment;

where s is half span;

and l, mean wing chord.

A positive control deflection corresponds to a negative airplane rotation. Thus:

η { Negative. . . . . .elevator pulled back
Positive. . . . . .elevator pushed forward

ζ { negative. . . . . rudder to starboard
positive. . . . . rudder to port

Thus in a right spin: $\eta < 0$, $\zeta < 0$ indicates that elevator and rudder are deflected in a spin-promoting sense.

Other symbols are explained in the text.

As regards the aerodynamic moments, the rolling moment $L_e = c_{L_e} F s q$ refers to the x_e axis, which with the tunnel axis forms the angle of yaw β_e (shown negative in fig. 3). The x_e axis is the track of the plane of symmetry of the model in the horizontal plane of the wind tunnel*. The pitching moment $M = c_M F l q$ is referred to the y transverse axis passing through the center of gravity. The conversion is based on a position of center of gravity 16 percent back from the mean wing chord - i.e., at a distance $2b/3\pi$ from the plane of symmetry - the position at which the flight tests were made. The yawing moment $N_e = c_{N_e} F s q$ is the aerodynamic moment about the z_a axis (lift axis). For purposes of comparison with the flight-test data, the yawing moment $N = c_N F s q$ about the normal axis was also computed** (fig. 13).

TEST DATA

a) Air Forces

The height of the measured maximum lift in consideration of the low Reynolds Numbers was very satisfactory. This is important for the present measurements in view of

---

*In all plots and in the text, the angle of attack is expressed as α_e and the angle of yaw as β_e, the subscript e indicating "experimental" and also "English." α is identical with α_c and β_e, as seen on comparing figs. 2 and 3. The different definition - resulting from the aerotechnical standards - was, however, retained in order to prevent a mix-up at the present stage of transition where the old systems of axes are still being employed.

** $N = N_c \cos \alpha_c + L_e \sin \alpha_c$; note the wrong sign in L. Hopf's "Aerodynamik," vol. 1, p. 270.

the relation of rolling moments to lift distribution. U.S. airfoil tests made in the high-pressure tunnel at large Reynolds Numbers give 1.47 as maximum lift coefficient for airfoil section 4418. This figure is considered too high because of the strong turbulence for which that tunnel is known.

The polar measurements (fig. 4) made at increased dynamic pressure wherein the effect of the laterally incident wind was explored over a large range of angles of yaw (to $\beta_e = 30^\circ$) disclosed the following:

1. Below maximum lift, the gradient $\frac{\partial c_a}{\partial \beta_e}$ decreases with increasing angle of yaw β_e; this decrease is correspondingly greater than product $\frac{\partial c_a}{\partial \beta_e}_{\beta_e=0} \times \cos \beta_e$;

2. As the angle of yaw increases the lift maximum shifts to higher α_e, with scarcely any change in $c_{a_{max}}$ (slipping);

3. The marked drop in c_a, after reaching maximum, moderates with increasing angle of yaw.

The effect of rolling on lift and drag is illustrated in figure 5 for two different angles of yaw (0 and 5 percent outward slip).

The originally existent left peak flattens out as the rate of rolling increases; in the high stalling range, the lift is practically unaffected by rolling. Of interest is the drop in drag at small angles of attack due to rotation; this is due to the fact that the half struck from below receives a higher lift - in relation to the momentary local flow direction - than the half struck from above. Since the greater lift is inclined slightly toward the nose of the airfoil, the sum of the projections on the mean flow direction yields a force directed against the flow and hence a decrease in drag. This phenomenon is intensified as soon as the local lifting force on the half struck at reduced angles of attack is directed downward; for in this case the lift projections acting against the mean flow direction become additive in equivalent wing sections (at distance $\pm y$ from the plane of symmetry).

On the other hand, since the tests in the range far beyond stalling disclose a distinct increase in drag with increasing rate of rolling, the effect of the different geometric orientation of the individual wing sections is investigated in the following, at least as to the order of magnitude.

According to figure 6, a wing strip of width l at distance y from the axis of rotation has a drag*

$$W(y) = \left\{ \overline{c}_w(\alpha_o + \alpha_\omega)\cos\alpha_\omega - \overline{c}_a(\alpha_o + \alpha_\omega)\sin\alpha_\omega \right\} l(y)\, l\, q_{res}$$

In view of the intended comparison with the experimental data, it may be considered as sufficient to neglect the induced angle of attack and to use for $\overline{c}_w$ and $\overline{c}_a$ the well-known coefficients c_{wo} and c_{ao}, ascertained in polar measurements for the particular wing at $\lambda = 0$.

These omissions give after a few changes the simple term for c_w as follows:

$$c_w \approx \frac{\Lambda}{4} \int_{-1}^{+1} \frac{c_{wo}(\alpha_o + \alpha_\omega)\cos\alpha_\omega - c_{ao}(\alpha_o + \alpha_\omega)\sin\alpha_\omega}{\cos^2\alpha_\omega} \frac{l(y)}{s}\, d\left(\frac{y}{s}\right)$$

From this presentation, it is seen that, at small airflow angles and average rotation values, the second summand below the integral produces a considerable decrease in total drag merely for kinematic reasons (angle of attack and dynamic pressure changes); for on the half struck from below, c_a is substantially greater than c_w, hence the term with $\sin\alpha_\omega$ is not negligible in relation to $\cos\alpha_w$ term. On the other half, the lift may of course be smaller than the drag, but the product $c_a \sin\alpha_\omega$ remains positive because of the reversal of the lift sign. Calculations yielded for $\alpha_o = -4^\circ$ and $\lambda = 0.37$, a 66-percent reduction in drag coefficient; the wind-tunnel tests showed the same reduction (fig. 5).

With stalled wing, the drag-decreasing effect of the second term of the sum is lost, as the pertinent lift-components in equivalent wing strips cancel approximately; the

---

*Quantity $\alpha_o + \alpha_\omega$ is here as elsewhere to be considered as argument.

drag-increasing effect of the first term of the sum becones so much more potent. The conditions are particularly simple when assuming the c_a curve to be a parabola as far as α_{max} and then a straight line in the stalling range. In a comparison of identical wing strips at positive rotation, a starboard drag increase defines an exactly identical port drag decrease, to the extent that both strips are coordinated to effective angles of attack belonging to the straight branch of the c_w curve. But if, in this example, the port wing strip achieves an angle of attack belonging to the curved part of the drag curve, the drag decrease is less; a rise in total drag is associated with it then. - A calculation for $\alpha_o = 25^\circ$ and $\lambda = 0.37$ yielded a 10-percent drag increment, which is in good agreement with the experimental results.

Accordingly, these arguments have indicated the following:

1. Rolling at low angles of attack decreases the drag;

2. In the stalling range the drag is increased by rolling; this increase is due to the difference $\alpha_o - \alpha_{max}$, the magnitude of rotation and the form of the wing (on a rectangular wing the effect is probably greater than on a triangular wing, because of the larger total drag contribution of the outer parts).

The absolute amount of the lateral force remains in most flight stages small compared to the lift. But in a study of spinning, a more accurate knowledge of the aspect of c_q may become necessary, since in the mathematical treatment of the spin the lateral force coefficient frequently occurs additively coupled with small quantities.

At small angles of attack, the measurements up to near the angle of α_{max} disclose a rise in lateral force of $\frac{\partial c_q}{\partial \beta_c} = -0.4$, almost independent of α_o (cf. fig. 7, where, to simplify matters, only the curve of c_q for one angle of sideslip is plotted).

In the zone beyond stalling, the reversal of sign of the lateral force is exceptional. It is due to the fact that at greater angles of air flow, the wing acts as brake disk, which causes an aerodynamic force in the direction of the advanced half of the wing.

The effect of rotation on the lateral force proves to be quite considerable. In absolute magnitude within the zone of a steady vertical spin (between 25° and 35° α under normal load) it remains, however, so small that, for the angle of yawed flow, for instance, it amounts to around 80° to 90°.*

b) Moments

The measurements of the pitching moment (fig. 8) manifest, in accordance with the opinions voiced in the literature, regarding the effect of yawing and rotation, no abnormal dependence on the two parameters. Still, the longitudinal moment is a little more influenced by lateral incident wind than by rotation about the wind axis. In figure 8, the moment coefficient c_M referred to the airplane center of gravity at three definite control settings is shown for an outward slip of $\beta_e = 10°$ at various rates of rotation. The curves are substantially parallel, since the normal force coefficients of a horizontal tail surface at different control deflections differ in general merely by an additive constant.

Numerical comparison of control effectiveness with theory is quite satisfactory; in the normal flight range the measurement for an elevator deflection of $\eta = \pm 30°$ gives a normal force coefficient ($q_H = q$ assumed for simplicity)

$$c_{n_H} = \frac{c_{M_o} F l}{F_H l_H} = \frac{0.45 \times 14.78 \times 1.34}{2.77 \times 4.00} = 0.80$$

the value for c_{M_o} being read from figure 8, the others from the airplane dimensions.

The theory gives approximately the same value for the normal force: the horizontal control surface of the M 27 b_1 has as aspect ratio of $\Lambda = 3.7$, hence $\frac{\partial c_{n_H}}{\partial \alpha_H} = 6$; with a control area of around 38 percent the value is around

*This figure is readily deduced from a relation for the angle of yaw based on the steady spin.

$0.7\sqrt{0.38} = 0.43$ for $\frac{\partial \alpha_H}{\partial \eta}$ with elevator hard up; the factor 0.7 for fully deflected control corresponds to the usual assumption respecting the the incipient loss of control effectiveness. Hence the normal force coefficient is

$$\Delta c_{n_H} = \frac{\partial c_{n_H}}{\partial \alpha_H} \frac{\partial \alpha_H}{\partial \eta} \Delta \eta = 0.006 \times 0.43 \times 30 = 0.78$$

Figure 9 shows for $\lambda = 0$ the yawing-rolling moment plotted against the angle of attack; below the stall this moment is small, depending particularly upon the shape of the wing tip and the dihedral. On approaching the stalling angle the yawing-rolling moment increases considerably, its maximum rise being coincident with the position of maximum lift. One salient feature is the large amount of the yawing-rolling moment in the region well beyond stalling. Since high lateral stability makes the steady spin very stable against small disturbances this fact is of importance for spinning investigations. The value of $\frac{\partial c_{L_e}}{\partial \beta_e} \approx 0.4$ established here is in good agreement with those reported elsewhere in the literature; for the yawing-rolling moment in the separated zone appears to be very little dependent on the design of the wing and on the dihedral angle, because its high amount is largely due to the transport of boundary layer material toward the rearward shifted wing tip.

In the prediction of the yawing-rolling moment, it was found that, at the small angles of attack $\frac{\partial c_{L_e}}{\partial \beta_e}$ is dependent on the angle of yaw, while the moment is constant over a large angle of yaw range in the stalled zone. As to the effect of the parameter of rotation on lateral stability, the measurements permit as yet of no definite appraisal.

The effect of the rotation about the wind axis on the rolling moment is shown for $\beta_e = 0^\circ$ and 10° (outward slip) in figures 10 and 11. For the non-stalled range, the measurements give a damping value in roll of $\frac{\partial c_{L_e}}{\partial \frac{\omega_{x_a} s}{v}} \approx -1.0$. The calculation of the pertinent tapered

wing by Multhopp's theory gives the same amount.

Instability in roll at stall and recurrence of damping in roll at high angles of attack and higher rolling velocities is well reproduced in the measurements. This damping in roll accompanying the spin is approximately half as great as that at small angles of attack and small λ.

A comparison of figures 10 and 11 discloses the well-known increase in autorotation velocity for outward slip. Measurements at 5° inward slip (not reproduced here) bring out the spin-retarding effect of the inward slip and hence the importance of the yawing moments.

The rise of the rate of autorotation in an outward slip is chiefly due to a movement of the boundary layer masses toward the rearward wing tip. This movement takes place in the rotating air stream against the rise of the static pressure, from which it may be concluded according to the measurements that, up to the employed rotation values of $\lambda = 0.37$ at least, the influence of the static pressure gradient is not excessively disturbingly effective on the boundary layer movement caused by yawing.

The damping in roll is not affected by elevator or rudder deflections, according to the experiments; the lever arm from rudder to wind axis is not abnormally great, even at higher angles of attack. Interesting aileron deflection experiments could not be made on the model.

While the rolling moment is largely caused by the wing, the yawing moment is due in approximately equal proportions to wing, fuselage, and lateral control surface, which, in addition, may even have different signs. Hence the limited instrumental accuracy expected beforehand in the prediction of the yawing moments, especially of the generally small yawing moments in rolling.

Figure 12 gives the yawing-moment curves without rotation; note, with rudder deflection the blanketing effect of the rudder by the elevator and stabilizer in the stalled range. This blanketing effect is intensified if accompanied by pushed-down elevator (not shown) even at small flow angles, so that the rudder effect drops 60 percent. In a side wind at very small angles of attack, a slight restoring yawing moment (curve $\beta = 10°$, $\zeta = 0°$) is created in consequence of the wind vane stability.

On approaching the stall the unstabilizing wing yawing moment increases considerably, and the directional stability is lost; the flow on the shoved-back wing tip breaks away sooner as a result of the accumulation of boundary layer material than on the half shoved forward. At further increasing angle of attack the amplified wing yawing moment is gradually superseded by the lateral control surface moment turning into the wind, although weakened as a result of the blanketing effect. The accuracy in the yawing moment measurements left much to be desired in consequence of the cases previously described

For the purposed comparison with the flight tests in figure 13, the yawing moment coefficients about the normal airplane axis are therefore plotted for several angles of attack between 15° and 40° with spin promoting control deflections against the spinning factor λ and $\beta_e = 0$; if accompanied by a positive angle of slip (outward) the points of intersection of the curves with the c_N zero axis shift toward the right.

A complete reproduction of the test data was foregone for the stated reasons, although qualitatively it was possible to include the effect of rolling on the yawing moment. (Thus it afforded a negative yawing moment in roll in the zone below the stall.) Hence it is logical to expect a satisfactory determination of the yawing moment in the rotating tunnel jet with greater instrumental accuracy (higher dynamic pressure, use of larger model). For, while the existence of a static pressure gradient may cause a movement of the boundary layer mass, it cannot create a wing yawing moment with linear superposition. The same may be assumed to hold true for the fuselage and control surface yawing moment: the drag may perhaps be falsified at higher α_e as a result of an air force toward the jet center but not the drag difference of the port and starboard side.

FLIGHT TESTS

No complete numerical agreement can obtain between the model test data and those at full scale because of the scale effect. Even so, it has been proved in the foregoing that the effect of the five factors α, β, λ, η, and ζ has been reproduced substantially correctly in the wind-tunnel tests. With a view to establishing the

relative difference compared to flight tests and particularly to verify whether the model tests simulate approximately under the same conditions in a steady spin, a few experimental flights were made with the M 27b_1.

During these tests a so-called "automatic observer" developed by the DVL was installed in the airplane. It recorded three angular velocities about the three principal axes of inertia, the three normal accelerations in the direction of the three axes, the sinking speed and the engine r.p.m.

In a steady spin (to which is solely referred herein) the equality of the resultant air force with the resultant mass force gives

$$A^2 + W^2 + Q^2 = G^2 + (m \Omega^2 R)^2$$

With the equality of the forces in direction of the path tangent giving

$$W + G \sin \gamma = 0$$

the flight-path angle in the spin at between -75° and -90° and the lateral force consistently small numerically, it follows that the drag is approximately equal to the gross weight and the lift equal to the centrifugal force.

As stressed in the discussion of the lateral force measurements, the angle of the yawed flow in a steep spin is in general very great and approaches a right angle; owing to this, the angle of attack and the absolute amount of the angle of pitch are complementary with, here, satisfactory accuracy to a right angle, even if the angle of the flight path does not amount to -90°. Hence the angle of attack α is given by

$$\cos \alpha = \frac{\omega_x}{\Omega}$$

The angle of yaw β can be computed by means of the equations of motion. A simpler way is, as was done in these flights, to measure β by means of a bent nozzle; according to the flight records β ranged at between 0° and 5° outward slip.

With b_x, b_y, and b_z denoting the measured normal

accelerations of the airplane, the force equilibrium gives

$$b_x^2 + b_y^2 + b_z^2 = g^2 + (\Omega^2 R)^2$$

from which the circumferential speed ΩR, the radius of spin R and the flight path angle γ can be determined.

Various pertinent airplane data during the flight tests follow:

$G/F = 46$ kg/m^2, wing loading

$i_x = 1.17$ m, radius of inertia about x axis

$i_y = 1.43$ m, radius of inertia about y axis

$i_z = 1.75$ m, radius of inertia about z axis

$x_s = 0.16\ l_m$, c.g. position back

The above table illustrates several test flights. Flights 1 and 2 are left spins, flight 3, a right spin; they must differ even by perfect airplane symmetry, since the gyroscopic yawing moment of a single-engine airplane, due to the propeller, is not negligible. Further differences are caused by the difficulty of keeping the controls ($\xi \approx 0°$, $\eta \approx -30°$, $\zeta \approx -30°$) at identical deflections during the tests.

	Flight 1	Flight 2	Flight 3
λ . . .	-0.47	-0.57	0.55
α [°] .	27.5	32.2	24.5
c_a . . .	1.17	1.38	1.29
c_w . . .	.50	.63	.56
c_M . . .	-.31	-.45	-.33
$c_L \times 10^3$	-3.2	-5.7	4.3
$c_N \times 10^3$	-4.0	-5.9	5.9

Since the spin factor λ could not be raised above 0.37 in the model tests, any extrapolation above this figure - for purposes of comparison with the flight test data - must be made with the reservation that on the boundary layer an airplane spinning at higher rates of rotation is not pressed outward by the inertia forces to such an extent as to cause a substantial change of the profile characteristics.

In a comparison of the values in the above tabulation with those from the model tests the high lift coefficients of the test flights, not even approximately approached in model tests, stand out. Wind-tunnel tests with elevator pulled back yielded lift coefficients of from 0.96 to 1.00 in the far range beyond the stall. However, the following should be noted: The wind-tunnel measurements themselves indicate a certain increment of c_a in several cases (compare fig. 5); because, since in first approximation it may be assumed that

$$c_a \approx \frac{\Lambda}{4} \int_{-1}^{+1} \frac{c_{a_0}(\alpha_0 + \alpha_w)\cos\ \alpha_w + c_{w_0}(\alpha_0 + \alpha_w)\sin\ \alpha_w}{\cos^2\ \alpha_w} \frac{t(y)}{s}\, d\left(\frac{y}{s}\right)$$

under the same premises as before, there is a possibility that at higher rates of rotation the lift itself may increase as a result of locally changed flow conditions. Then again, it may be a case of insufficient instrumental accuracy available in the free-flight measurements. But a definite answer to these questions must be held in abeyance pending additional flight test data. Installation of improved equipment in the automatic observer now under way should afford more satisfactory lift coefficients in flight.

Compared with the values of figure 5, the drag coefficients recorded in flight are, on the whole, lower than for the model tests in spite of the higher rotation values. This was, of course, as expected, since the scale effect is very noticeable then.

The pitching-moment coefficients obtained from the flights are, on the other hand, in satisfactory agreement with the curves of figure 8.

An appraisal of the roll- and yawing-moment coeffi-

cients requires the most exact knowledge of the magnitude of the angle of yaw; here some improvement is anticipated for the future tests. Because these two moments are not measured about model-fixed axes in the wind-tunnel tests, some correction is necessary for a comparison with flight test data. If this is effected for an angle of attack of 25° on the basis of a 5° outward slip, the extrapolation carried out under the earlier reservation of a rotation somewhat above 0.4, discloses an equilibrium condition, if both the elevator and the rudder are fully deflected in the spin promoting sense. So, within a certain degree of accuracy, the wind-tunnel data for the rolling and yawing moment may also be considered to be agreeable with the flight test data.

Translation by J. Vanier,
National Advisory Committee
for Aeronautics.

REFERENCE

1. Kramer, M., and Krüger, K. B.: A New Spinning-Test Method. T.M. No. 859, N.A.C.A., 1938.

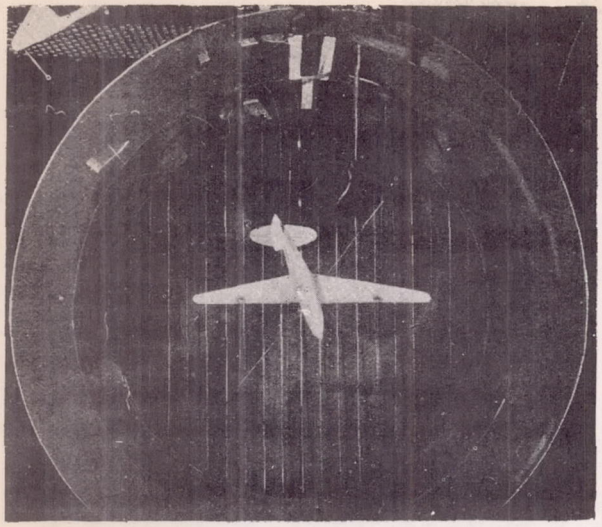

Figure 1.- Experimental set up with model mounted.

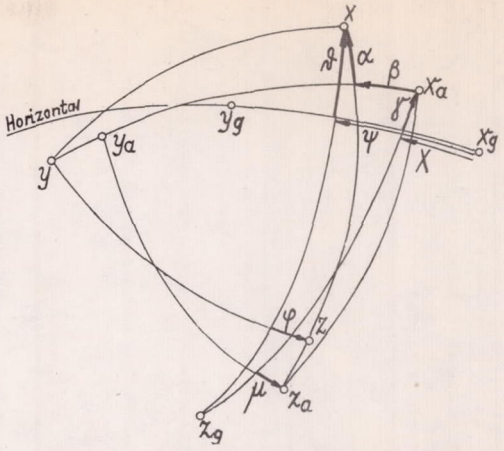

Figure 2.- Coordinate system.

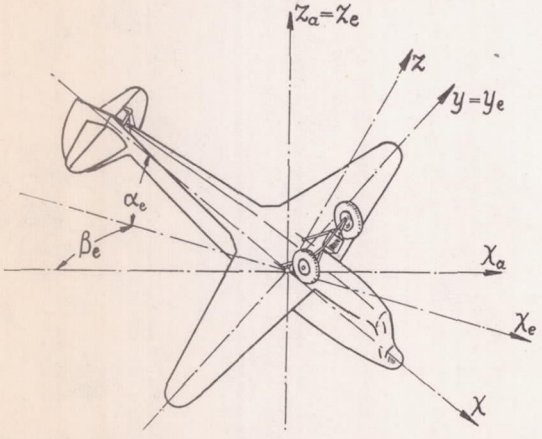

Figure 3.- System of axes.

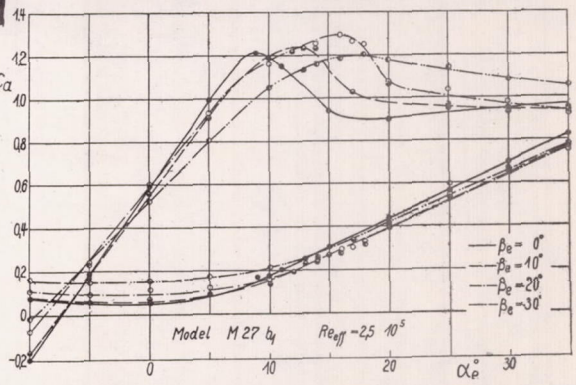

Figure 4.- Effect of yaw on lift and drag.

$$\lambda = \frac{\omega s}{v_0}$$

$$v_{res} = v_0\sqrt{1+\left(\lambda\frac{y}{s}\right)^2}$$

$$\alpha_\omega = arc.tg\left(\lambda\frac{y}{s}\right)$$

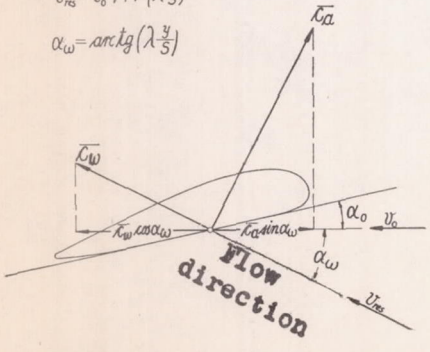

Figure 6.- Change of drag during rolling.

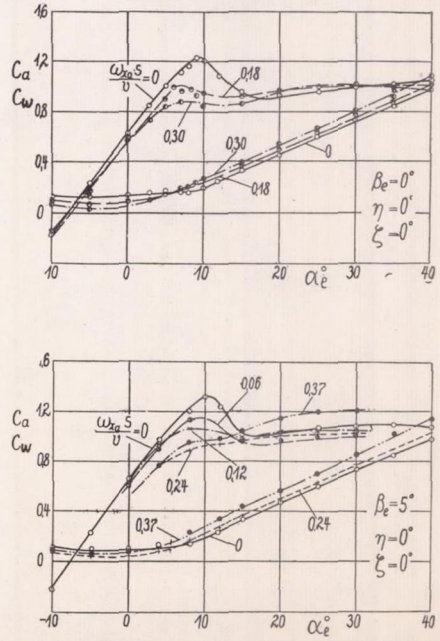

Figure 5.- Lift and drag coefficient plotted against rate of rolling.

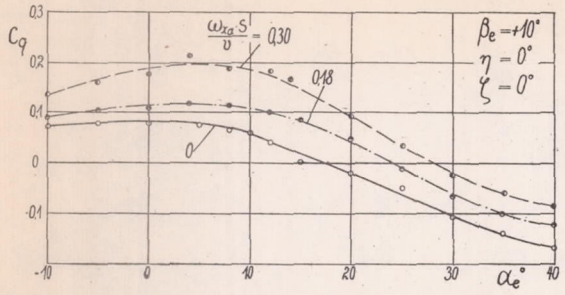

Figure 7.- Coefficient of lateral force at 10° angle of yaw.

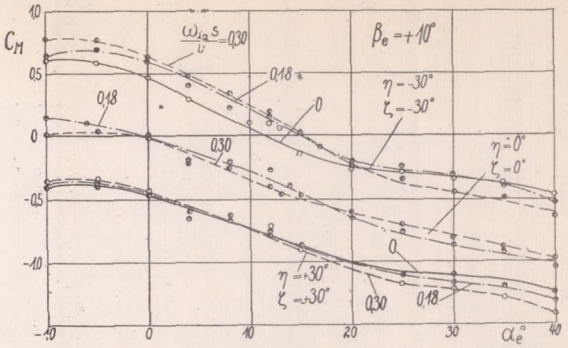

Figure 8.- Coefficient of pitching moment at different control deflections.

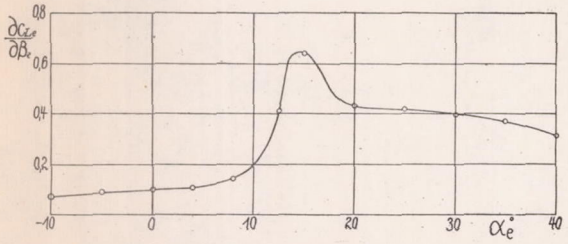

Figure 9.- Rolling moment in yaw against angle of attack α_e.

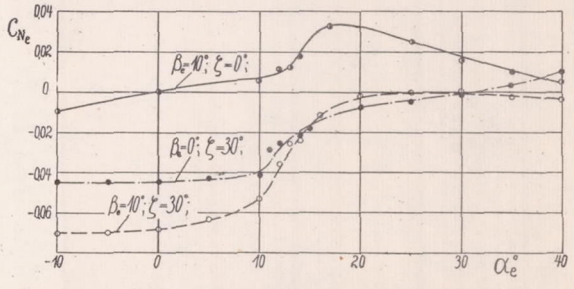

Figure 12.- Coefficient of yawing moment at different control settings.

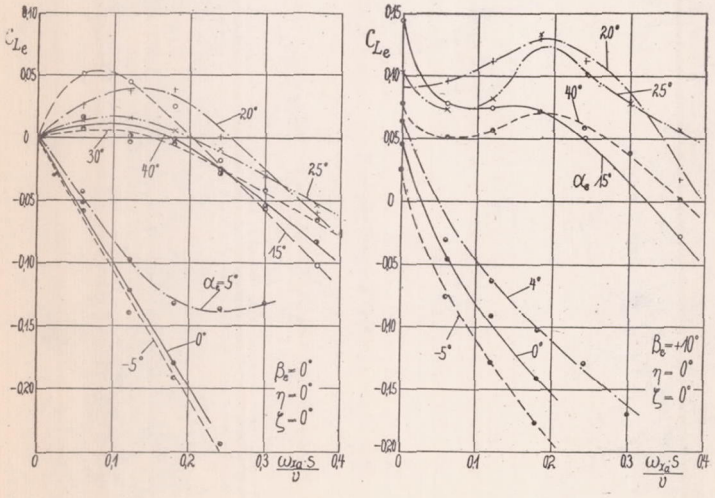

Figure 10-11.- Coefficient of rolling moment against $\frac{\omega_{xa} s}{v}$, for $\beta_e = 0°$ and $\beta_e = 10°$.

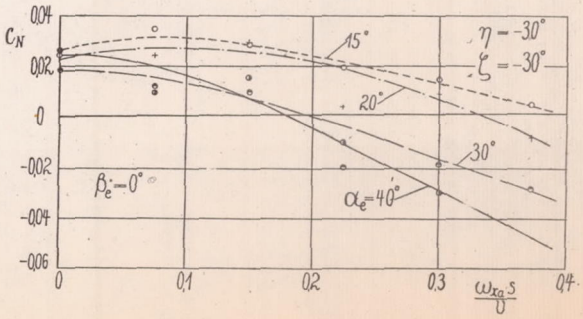

Figure 13.-.Coefficient of yawing moment against $\frac{\omega_{xa} s}{v}$, at $\beta_e = 0°$.